Proc. Of the 4th International E-Conference on Advances in Engineering, Technology and Management - ICETM 2021

ISBN: 978-1-63248-191-7 DOI: 10.15224/978-1-63248-191-7-01

Effect of magnet particles deposited in cathode side on oxide fuel cell performance

[Abir Yahya , Hacen Dhahri, Khalifa Slimi]

***Abstract*— A two-dimensional model based on the lattice Boltzmann method (LBM) is established to study the performance of solid oxide fuel cell (SOFC). A single phase multicomponent model is used to describe mass transport in the porous electrodes and fuel/air channels. Our results are compared with those from the literature and a good agreement is found. After model validation a parametric analysis is conducted to examine the effect of operating parameters on SOFC performance. The purpose of this paper is to examine the effect of the Kelvin force, caused by magnet particles deposited on cathode/electrolyte interface, on SOFC performance. The obtained results suggest that no magnetic field effect was observed for SOFC performance.**

***Keywords*— SOFC performance, multicomponent flow, Magnetic field gradient, Kelvin force**

I. Introduction

The SOFC performance is directly related to properties of the electrode materials and impurities in the fuel [3–7]. Several researches aimed to increase the performance of SOFC by exploring new materials and optimizing the cell structure [8–11]. Recently, Ruksawong et al. [12] have studied experimentally the effect of a magnetic field on water transport in PEMFC in terms of performance enhancement. Also, the effect of a magnetic field directly applied to a PEMFC have been investigated by Matsushima et al. [13]. The results showed that at lower partial pressure of oxygen gas and higher current densities, the performance of the fuel cell is improved or is deteriorated depending on de direction of the magnetic field.

Abir Yahya
Thermal and Energetic Systems Studies Laboratory, National Engineering School,
Monastir University, Ibn Eljazzar Street, 5019, Monastir, Tunisia
e-mail

Hacen Dhahri
Thermal and Energetic Systems Studies Laboratory, National Engineering School,
Monastir University, Ibn Eljazzar Street, 5019, Monastir, Tunisia

Khalifa Slimi
Higher Institute of Transport and Logistics, University Sousse,
Riadh City, P.O.Box 247, 4023, Sousse, Tunisia.

Because, it is substantially difficult to measure experimentally the phenomena taking place inside the SOFC stacks due to their high operating temperature, numerical simulation as an economic approach was developed to identify an optimal design of SOFC. Most of the models are used to predict the flow, the temperature and the current distributions [14-18].

The lattice Boltzmann method (LBM) is a powerful numerical technique based on kinetic theory for simulating fluid flows and modeling the physics in fluids. The LBM is second-order accurate in time and space, which is sufficient for most engineering applications. As the boundaries are appropriately treated with this method, makes LBM competitive for complex domain geometries such as porous media [19, 20]. A general numerical scheme based on LBM was established to investigate coupled multiple physicochemical thermal processes at the pore-scale [21], to simulate a thin anode (50 mm) of Ni-metal/YSZ-electrolyte cermet for a high-temperature electrolyte supported SOFC [22] and to develop an electrochemical model to predict the performance of an anode-supported SOFC [23]. A pore scale Lattice Boltzmann (LB) model is developed to predict the mass transfer, reforming, electrochemical reactions and carbon deposition in the porous anode of a solid oxide fuel cell (SOFC) fed with methane [24].

In this work, a two-dimensional LB model of non-isothermal planar SOFC was developed to study the multicomponent gases transport in the channels and porous electrodes. An electrochemical model is also established to study the performance of a planar anode supported solid oxide fuel cell. To demonstrate the capabilities of the developed model, simulations are conducted to predict the operating voltage effect on hydrogen and oxygen molar fractions distributions and the cell temperature distribution. The effect of operating temperature on the cell voltage and power density is also examined. Moreover, the developed model permits us to examines the effect of a magnetic field gradient that is applied in the cathode/electrolyte interface by depositing Nd-Fe-B permanent particles.

II. SOFC Model governing equations

SOFCs are built up of an electrolyte sandwiched between an anode and cathode. Figure 1 shows the general operation of a SOFC.

Proc. Of the 4th International E-Conference on Advances in Engineering, Technology and Management - ICETM 2021

ISBN: 978-1-63248-191-7 DOI: 10.15224/978-1-63248-191-7-01

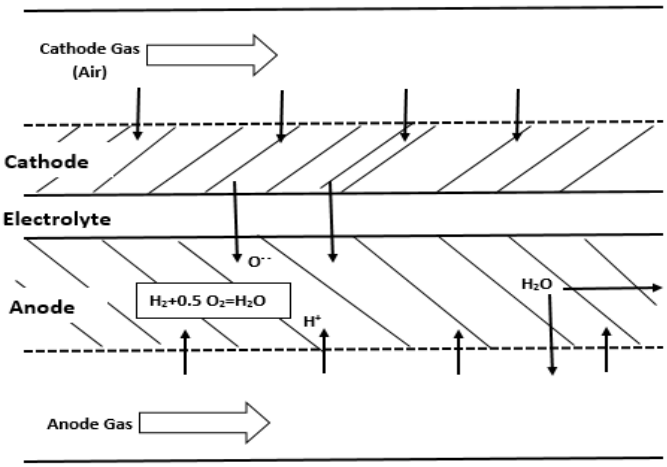

Figure 1.Schematic of the computational domain of a planar SOFC.

As can be seen from Fig.1, oxygen gets pumped into the cathode side where it reacts with the catalyst and electrons to reduce into oxygen ions (O2). The electrolyte conducts oxygen ions from the cathode side to the anode side. Here the fuel is pumped in and becomes oxidized, by the oxygen ions, to form water and electrons. These electrons then get forced through the interconnect from the anode to the cathode which generates an electric current [25].

A. *Electrochemistry of SOFC*

Taking into account all the overpotential effects in a solid oxide fuel cell, the cell potential is given by [26].

$$V_{cell} = E - \eta_{act,a} - \eta_{act,c} - \eta_{con,a} - \eta_{con,c} - \eta_{ohmic} \quad (1)$$

where E, $\eta_{act,a}$, $\eta_{act,c}$, $\eta_{con,a}$, $\eta_{con,c}$ and η_{ohmic} are the equilibrium voltage, the activation overpotential of the anode, the activation overpotential of the cathode, the concentration overpotential of the anode, the concentration overpotential of the cathode and the ohmic overpotential.

The equilibrium voltage of a SOFC can be expressed by the Nernst equation

$$\mathrm{E} = E_0 + \frac{RT}{2F}\ln\left(\frac{P^0_{H_2}\left(P^0_{O_2}\right)^{\frac{1}{2}}}{P^0_{H_2O}}\right) \quad (2)$$

The ohmic and activation terms can be calculated using the same method described in our previous work [27] and the partial pressures are calculated from the molar fraction.

The concentration overpotential can be expressed as a function of the gas concentration difference between the porous electrode surface and the electrode-electrolyte interface [23].

$$\eta_{con,a} = -\frac{RT}{2F}\ln\left(\frac{Y_{H_2O,bulk}\,Y_{H_2,a/e}}{Y_{H_2,bulk}\,Y_{H_2O,a/e}}\right) \quad (3)$$

$$\eta_{con,c} = -\frac{RT}{2F}\ln\left(\frac{Y_{O_2,a/e}}{Y_{O_2,bulk}}\right)^{\frac{1}{2}} \quad (4)$$

B. *Fluid flow problem*

The fluid flow is governed by Navies Stokes equation [28]:

$$\frac{\partial(\rho U)}{\partial t} + \frac{\partial(\rho U U)}{\partial x} + \frac{\partial(\rho V U)}{\partial y} = -\frac{\partial(P)}{\partial x} + \frac{\partial}{\partial x}\left(\mu\frac{\partial U}{\partial x}\right) + \frac{\partial}{\partial y}\left(\mu\frac{\partial U}{\partial y}\right) + S_x \quad (5)$$

$$\frac{\partial(\rho V)}{\partial t} + \frac{\partial(\rho U V)}{\partial x} + \frac{\partial(\rho V V)}{\partial y} = -\frac{\partial(P)}{\partial x} + \frac{\partial}{\partial x}\left(\mu\frac{\partial V}{\partial x}\right) + \frac{\partial}{\partial y}\left(\mu\frac{\partial V}{\partial y}\right) + S_y \quad (6)$$

The source terms Sx and Sy are determined by Darcy's law for both anode and cathode [29]:

$$S_x = -\frac{\mu}{k}\varepsilon U \quad (7)$$

$$S_y = -\frac{\mu}{k}\varepsilon V \quad (8)$$

Where k is the permeability of the porous electrodes, ρ is the density, ε is the porosity and μ is the dynamic viscosity.

C. *Heat transfer problem*

The local temperature equilibrium was assumed to account for the temperature of fluid and solid phases in the porous electrodes. The dominating phenomena in this model are heat convection and heat conduction.

The total energy conservation equation in cartesian coordinates system writes:

$$\frac{\partial\left[(\rho c_p)_{eff}T\right]}{\partial t} + \frac{\partial\left[(\rho c_p)_{eff}UT\right]}{\partial x} + \frac{\partial\left[(\rho c_p)_{eff}VT\right]}{\partial y} = \frac{\partial}{\partial x}\left(\lambda_{eff}\frac{\partial T}{\partial x}\right) + \frac{\partial}{\partial y}\left(\lambda_{eff}\frac{\partial T}{\partial y}\right) + S_T \quad (9)$$

- ***Joule heating***

Due to the existence of resistance for ions transferring through the electrolyte and electrons through the cell's anode and cathode, heat generates by the ohmic heating can be calculated as follows:

$$S_J = \sum R_{ohm}\,J^2 \quad (10)$$

Where J denotes the current density. R_{ohm} is the total area specific resistance that can be expressed as follows [30,31] :

$$R_{ohm} = \frac{d_a}{\sigma_a} + \frac{d_c}{\sigma_c} + \frac{d_e}{\sigma_e} \quad (11)$$

Proc. Of the 4th International E-Conference on Advances in Engineering, Technology and Management - ICETM 2021

ISBN: 978-1-63248-191-7 DOI: 10.15224/978-1-63248-191-7-01

where d_a, d_c and d_e are the thickness of anode, cathode and electrolyte, respectively; σ_a, σ_c and σ_e are the electrical and ionic conductivities of the SOFC components [31,32] .

- ***Chemical reaction heat***

Due to entropy creation due to the electrochemical reactions at the anode-electrolyte interface, the heat generation is determined as [31]:

$$S_r = \frac{T\Delta S}{2F} J \tag{12}$$

where ΔS is the reaction entropy variation expressed as [33]:

$$\Delta S = \Delta S_0 + \int_{298}^{T} \frac{\Delta C_{pr}}{T} dT \tag{13}$$

- ***Activation polarization heat***

Activation losses are controlled by the electrode kinetics at the reaction site, which are assumed to be located at the electrode-electrolyte interface. The expressions of the activation losses in the anode and the cathode are expressed according to the Tafel approach [34]:

$$S_{act} = J\eta_{act,i} \tag{14}$$

$$\eta_{act,i} = \frac{RT}{\alpha_i nF} ln\left(\frac{J}{J_{0,i}}\right) \tag{15}$$

where α_i is the transfer coefficient and $J_{0,i}$ is the exchange current density that represents the readiness of an electrode to proceed with electrochemical reaction. $J_{0,a}$ and $J_{0,c}$ can be expressed as [35]:

$$J_{0,a} = \frac{RT}{nF}\gamma_a exp\left(-\frac{E_{act,a}}{RT}\right) \tag{16}$$

$$J_{0,c} = \frac{RT}{nF}\gamma_c exp\left(-\frac{E_{act,c}}{RT}\right) \tag{17}$$

where $E_{act,a}$ and $E_{act,c}$ are the activation energy levels at the anode and cathode respectively; γ_a and γ_c are the coefficients for exchange current density for anode and cathode,respectively.

D. *Mass transfer problem*

Mass transfer in the flow channel and the porous electrodes is modeled using the following equation [28]:

$$\frac{\partial(\rho U Y_i)}{\partial x} + \frac{\partial(\rho V Y_i)}{\partial y} = \frac{\partial}{\partial x}\left(\rho D_{i,m}\frac{\partial Y_i}{\partial x}\right) + \frac{\partial}{\partial y}\left(\rho D_{i,eff}\frac{\partial Y_i}{\partial y}\right) + S_{i,m} \tag{18}$$

Where Yi is the mass fraction of species i and $S_{i,m}$ the mass source term that can be expressed by the species flux at the electrodes/electrolyte interfaces as:

$$S_{H_2} = \frac{JM_{H_2}}{2F} \tag{19}$$

$$S_{H_2O} = \frac{JM_{H_2O}}{2F} \tag{20}$$

$$S_{O_2} = \frac{JM_{O_2}}{4F} \tag{21}$$

E. *Boundary conditions*

It is required to give an accurate set of boundary conditions that depict the flow and reaction within the domain. The velocity, temperature, and mass fraction of species are specified at the inlet. Boundary conditions of zero gradient are applied for velocity, temperature and species mass fraction at the outlet. At the fuel channel/anode interface and at the air channel/cathode interface, boundary conditions that satisfy both temperature and heat flux continuity are used. A continuation of the flux terms for each species is also imposed. At the anode/electrolyte and cathode/electrolyte interfaces, where the electrochemical reactions take place, the flux terms for each species are equal to the surface reaction rates [15,17].

III. Numerical method

A. *Momentum equation*

The D_2Q_9 model, which consists of 9 distribution functions, has been used. The developed LBE of a density distribution function for the evolution of the velocity field is given as [36].

$$f_i(x + e_i\,\Delta t, t + \Delta t) - f_i(x,t) = -\frac{1}{\tau}\left[f_i(x,t) - f_i^{eq}(x,t)\right] + \Delta t F_i \tag{22}$$

where e_i is the discrete lattice velocity in direction i; F_i is the external force. τ denotes the lattice relaxation time, f_i^{eq} is the equilibrium distribution function and f_i is the density distribution function for the velocity field.

The equilibrium distribution function is expressed as:

$$f_i^{eq}(x,t) = w_i\rho\left[1 + \frac{e_i u}{c_s^2} + \frac{(e_i u)^2}{2\varepsilon c_s^4} - \frac{u^2}{2\varepsilon c_s^2}\right] \tag{23}$$

ISBN: 978-1-63248-191-7 DOI: 10.15224/978-1-63248-191-7-01

After evolving on the discrete lattices, the density and velocity can be calculated using

$$\rho = \sum_i f_i \tag{24}$$

$$\rho u = \sum_i e_i f_i \tag{25}$$

B. *Energy equation*

Based on the work of Jinku [37], the evolution equation for heat transfer can be generally given as,

$$g_i(x + e_i\,\Delta t, t + \Delta t) - g_i(x,t) = -\frac{1}{\tau_g}\left[g_i(x,t) - g_i^{eq}(x,t)\right] + \Delta t G_i \tag{26}$$

Where the equilibrium distribution is written as:

$$g_i^{eq}(x,t) = w_i T\left[1 + \frac{e_i u}{c_s^2}\right] \tag{27}$$

Jinku proposed an expression for the forcing term Q appearing in the energy equation:

$$G_i = w_i\left(1 - \frac{0.5}{\tau_g}\right)\frac{S_T}{\rho c_p} \tag{28}$$

Therefore, the temperature can be calculated from the following equation:

$$T = \sum_i g_i + \frac{\Delta t}{2}\frac{S_T}{\rho c_p} \tag{29}$$

C. *Mass equations*

For the single phase- multicomponent flow consisting of hydrogen and water vapor species, streaming and collision processes are solved individually for each species to find distribution function h_i^k on the basis of Shan and Chen model [38]. Here the superscript k denotes the kth chemical species and the subscript i denotes the velocity direction of a single-particle.

The general form of the lattice Boltzmann equation for a distribution function h_i^k in the BGK approximation is:

$$h_i^k(x + e_i\,\Delta t, t + \Delta t) = \omega_k h_{i,k}^{eq}(x,t) + (1 - \omega_k) h_i^k(x,t) \tag{30}$$

Where $\omega_k = \frac{1}{\tau_k}$, τ_k is the single relaxation time for each component related to the kinematic viscosity. $h_{i,k}^{eq}$ is the local equilibrium distribution function defined as :

$$h_{i,k}^{eq}(x,t) = \rho_k\, w_i\left[1 + \frac{e_i u'}{c_s^2} + \frac{(e_i u')^2}{2c_s^4} - \frac{u'^2}{2c_s^2}\right] \tag{31}$$

where u' is the common velocity in lattice units and ρ_k is the component density.

The component density and velocity are obtained:

$$\rho_k = \sum_i h_i^k \tag{32}$$

$$u_k = \frac{\sum_i h_i^k\, e_i}{\rho_k} \tag{33}$$

Then, the total density and common velocity are calculated by:

$$\rho_{total} = \sum_k \rho_k \tag{34}$$

$$u' = \frac{\sum_k \sum_i h_i^k\, e_i\, \omega_k}{\sum_k \rho_k \omega_k} \tag{35}$$

The mass fraction of each component is defined as follows:

$$Y_k = \frac{\rho_k}{\rho_{total}} \tag{36}$$

IV. Results and discussion

A. *Model validation*

The validation of our model is conducted based on the experimental results of Rogers et al. [39]. The used model parameters and cell dimensions to predict the distribution of temperature and molar fractions distributions are reported in Table 1.

The predicted results are plotted in Fig. 2 and are compared to the available experimental data. It is noted that a good agreement is found. Minor discrepancies between computational and experimental data are observed, which can be attributed to the unavailability of some geometrical aspects of the experimental system.

TABLE 1. SOFC model parameters used for validation on Rogers et al. [39] experiments

Parameter (Units)	Value
Fuel inlet temperature (K)	1073
Air inlet temperature (K)	1073
Fuel composition (_)	0.95/0.05
Operating pressure (atm)	1
Porosity (_)	0.375
Tortuosity (_)	1
Average pore radius (m)	$2.6\ 10^{-6}$
Fuel cell length (m)	0.016
Anode porous electrode width (m)	0.001
Cathode porous electrode width (m)	0.00005
Electrolyte width (m)	0.00001
Anode electrode conductivity (S m^{-1})	71 428.57
Cathode electrode conductivity (S m^{-1})	5376.34
Electrolyte conductvity (S m^{-1})	0.64
Anode pre-exponential coefficient (A m^{-2})	$1.344\ 10^{10}$
Cathode pre-exponential coefficient (A m^{-2})	$2.051\ 10^{9}$
Anode activation energy (J.$gmol^{-1}$)	$1\ 10^{5}$
Cathode activation energy (J.$gmol^{-1}$)	$1.2\ 10^{5}$

Proc. Of the 4th International E-Conference on Advances in Engineering, Technology and Management - ICETM 2021

ISBN: 978-1-63248-191-7 DOI: 10.15224/978-1-63248-191-7-01

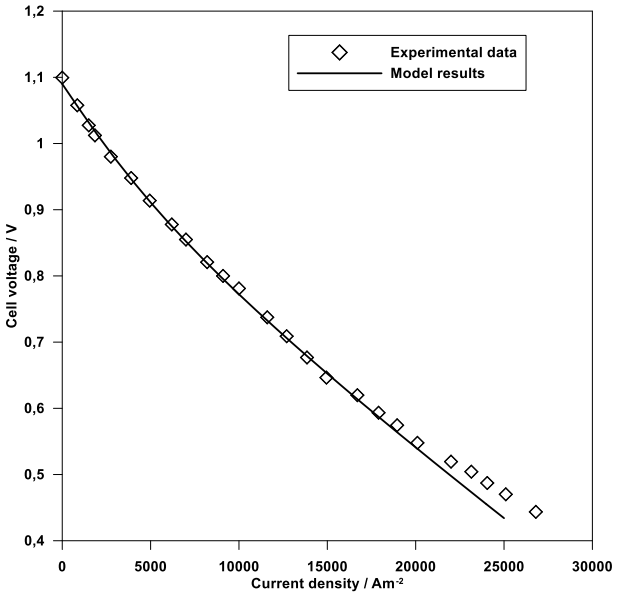

Figure 2. Comparison between the model results and experimental data

B. *Parametric analysis*

The parameters of the SOFC model and the input parameters of standard case are depicted in Table 2 and 3, respectively.

Using the input parameters reported in table 3, with an operating voltage of 0.6 V, the molar fractions of hydrogen and oxygen are depicted in figure 3. As hydrogen and oxygen flow in the fuel and air channel, respectively, they diffuse through the porous electrodes and they are consumed at the electrodes/electrolyte interfaces where the half-cell electrochemical oxidation and reduction reactions take place. Consequently, both H2 molar fraction and O2 molar fraction decrease from the inlet to the outlet of the cell. Since the diffusion in the porous electrodes is slower than in the fuel and air channels, the molar fraction gradients of hydrogen and oxygen in the anode and cathode are higher than in the gas channel.

TABLE 2.SOFC model parameters

Parameter (Units)	Value[15, 35]
Anode thermal conductivity ($Wm^{-1} K^{-1}$)	10 [15]
Fuel thermal conductivity ($Wm^{-1} K^{-1}$)	0.32 [15]
cathode thermal conductivity ($Wm^{-1} K^{-1}$)	11 [15]
Air thermal conductivity ($Wm^{-1} K^{-1}$)	0.58 [15]
Electrolyte thermal conductivity ($Wm^{-1} K^{-1}$)	2 [15]
Anode electrode conductivity (S m^{-1})	$\frac{9.5\ 10^{7}}{T} exp\left(-\frac{1150}{T}\right)$ [15]
Cathode electrode conductivity (S m^{-1})	$\frac{4.2\ 10^{7}}{T} exp\left(-\frac{1200}{T}\right)$[15]
Electrolyte conductvity (S m^{-1})	$3.34\ 10^{4} exp\left(-\frac{10300}{T}\right)$ [15]
Anode pre-exponential coefficient (A m^{-2})	1.344 10^{10}[35]
Cathode pre-exponential coefficient (A m^{-2})	2.051 10^{9}[35]
Anode activation energy (J.$gmol^{-1}$)	1 10^{5} [35]
Cathode activation energy (J.$gmol^{-1}$)	1.2 10^{5}[35]

TABLE 3. Input parameters of base case

Parameter (Units)	Value[23]
Fuel inlet temperature (K)	1123
Air inlet temperature (K)	1123
Fuel composition (_)	0.97/0.03
Operating pressure (atm)	1
Gas law constant (m^3 atm $gmol^{-1} K^{-1}$)	8.20575 10^{-5}
Faraday's constant (A s $gmol^{-1}$)	96,485.3
Permeability (m^2)	1.7 10^{-10}
Porosity (_)	0.46
Tortuosity (_)	4.5
Average pore radius (m)	2.6 10^{-6}
Anode porous electrode width (μm)	750
Cathode porous electrode width (μm)	50
Electrolyte width (μm)	50

The increase of the cell operating voltage leads to the decrease of the current density, which results in lower consumption rates of H2 and O2. As shown in figures 3 and 4, the molar fractions of hydrogen and oxygen are as higher as the cell operating voltage is higher.

Figure 5 illustrates the temperature distribution in the SOFC at operating potentials of 0.6 V and 0.4 V. The heat generated by the exothermic electrochemical reactions is transferred along the PEN structure mainly by conduction to the gas flow channels where it is transferred by convection. This is inducing an increase of temperature from the inlet to the outlet of cell. The temperature gradient of the cathode side is found to be slightly higher, as the thin cell cathode can transfer heat from the electrolyte to the air flow channel at a fast rate. Since the heat generation due to electrochemical reactions and irreversible overpotential losses depend on the current density, the temperature rises with the decrease of cell voltage.

C. *Effect of Kelvin force on the SOFC performance*

When a fluid is under external magnetic field H, the force per unit volume [40] is:

$$\mathbf{f} = \nabla p + \mu_0 \boldsymbol{M}.\nabla \boldsymbol{H} \qquad (37)$$

where $= \chi \boldsymbol{H}$, $\boldsymbol{B} = \mu_0 \boldsymbol{H}$, μ_0 is the permeability of vacuum (4π 10-7 Hm-1), χ is the magnetic susceptibility of fluid $\left(\chi_{O_2} = 1.91\ 10^{-6} \text{ at } 273\ \text{K}\right)$, p is the pressure and $\boldsymbol{B}$ is the magnetic flux density. The second term $\mathbf{f_m} = \mu_0 \boldsymbol{M}.\nabla \boldsymbol{H} = \frac{\chi}{\mu_0}\ \boldsymbol{B}.\nabla \boldsymbol{B}$ is the Kelvin force which trends to act on diamagnetic fluid such as water toward regions of lower magnetic fields and paramagnetic fluid such as oxygen gas toward higher magnetic fields.

A magnetic field gradient was applied around the interface between the cathode and the electrolyte by depositing Nd-Fe-B permanent particles. Based on the experimental study of Okaba et al [41], magnetic field is generated in y-direction near the interface. To obtain an equivalent magnetic field, we used the distribution of magnetic field strength along the central axis perpendicular to the pole surface of the cubic magnet [42].

Proc. Of the 4th International E-Conference on Advances in Engineering, Technology and Management - ICETM 2021

ISBN: 978-1-63248-191-7 DOI: 10.15224/978-1-63248-191-7-01

$$B(y) = \frac{B_r}{\pi}\left(\tan^{-1}\frac{ab}{a\,y\sqrt{a^2+b^2+4y^2}} - \tan^{-1}\frac{ab}{2(y+l)\sqrt{a^2+b^2+4(y+l)^2}}\right) \quad (38)$$

Where B_r is the residual flux density of the magnet, ab is the cross section of the magnet and l is the thickness of the magnet.

The magnetic force acting on nitrogen and water vapor is negligible because their magnetic susceptibilities are much smaller than that of oxygen [43]. Because Kelvin force is a body force similar to the gravitational force and assuming that B changes only on the y-direction, the gas-phase velocity can be expressed as:

$$u^g = -\frac{k}{\mu}\frac{\partial P}{\partial x}$$

$$v^g = -\frac{k}{\mu}\frac{\partial P}{\partial x} - \frac{k}{\mu}\frac{\chi}{2\mu_0}\rho x_o \frac{dB^2}{dy} \quad (39)$$

The simulated polarization and power density curves of single fuel cell including Nd/ Fe/B particles in the cathode side are illustrated in Figure 7, with and without magnetization of magnet particles. When the Kelvin force acts on the oxygen gas, the cell performance is the same as that without magnetization. This is explained by the non-effect of magnetic field in oxygen gas distribution as shown in Figure 6. Numerical simulation results showed reasonable agreement with the results of Wang et al [43] study when the magnet effect was investigated only on oxygen.

v. Conclusion

A 2D thermal-fluid model for a planar solid oxide fuel cell is developed. The model developed basing on lattice Boltzmann method is firstly validated with experimental results from literature. It is found that increasing the operating voltage leads to the increase of the hydrogen and oxygen molar fractions. Since the increase of the operating voltage leads to a decrease of the current density, the temperature rises with the decrease of cell voltage. The effect of magnetized magnet particles deposited in the cathode side on the SOFC performance is also investigated numerically. The obtained results show that the performance of the cell is not subordinate to the magnetization.

Proc. Of the 4th International E-Conference on Advances in Engineering, Technology and Management - ICETM 2021

ISBN: 978-1-63248-189-4 DOI: 10.15224/978-1-63248-191-7-01

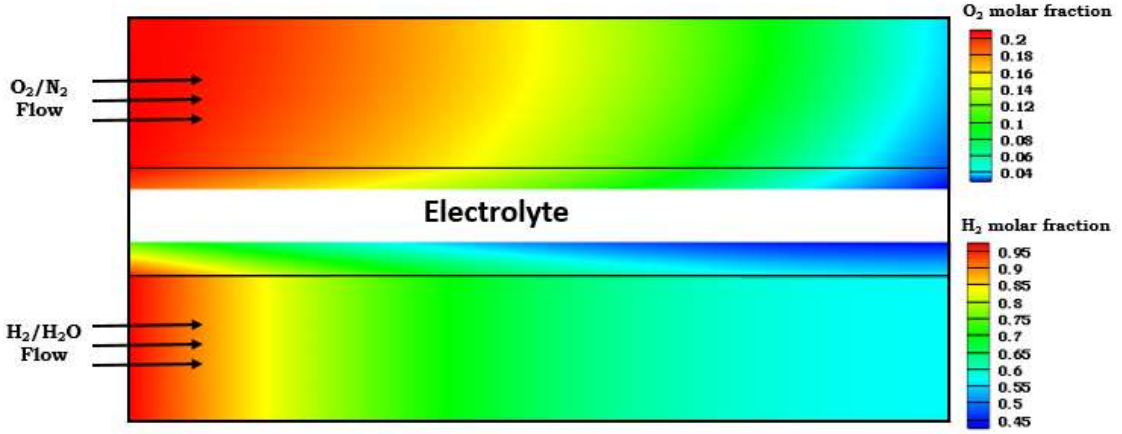

Figure 3. H2 and O2 molar fraction distribution at operating voltage 0.6 V

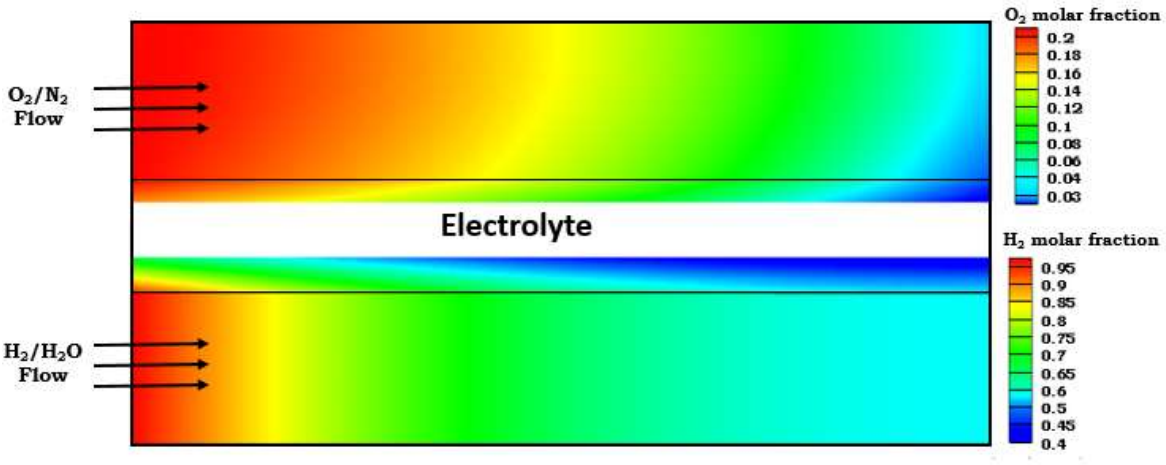

Figure 4. H2 and O2 molar fraction distribution at operating voltage 0.4 V

Proc. Of the 4th International E-Conference on Advances in Engineering, Technology and Management - ICETM 2021

ISBN: 978-1-63248-189-4 DOI: 10.15224/978-1-63248-191-7-01

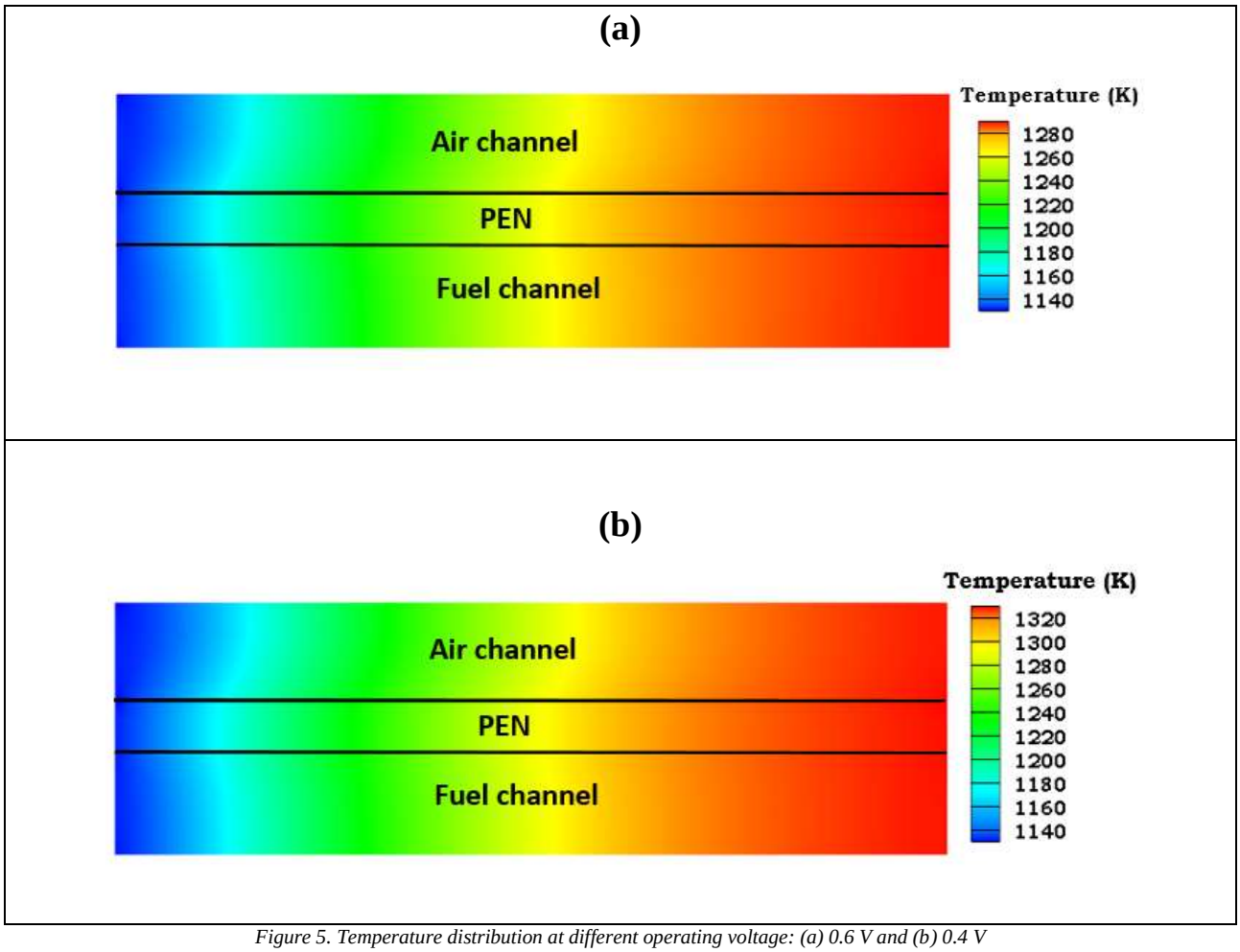

Figure 5. Temperature distribution at different operating voltage: (a) 0.6 V and (b) 0.4 V

Proc. Of the 4th International E-Conference on Advances in Engineering, Technology and Management - ICETM 2021

ISBN: 978-1-63248-189-4 DOI: 10.15224/978-1-63248-191-7-01

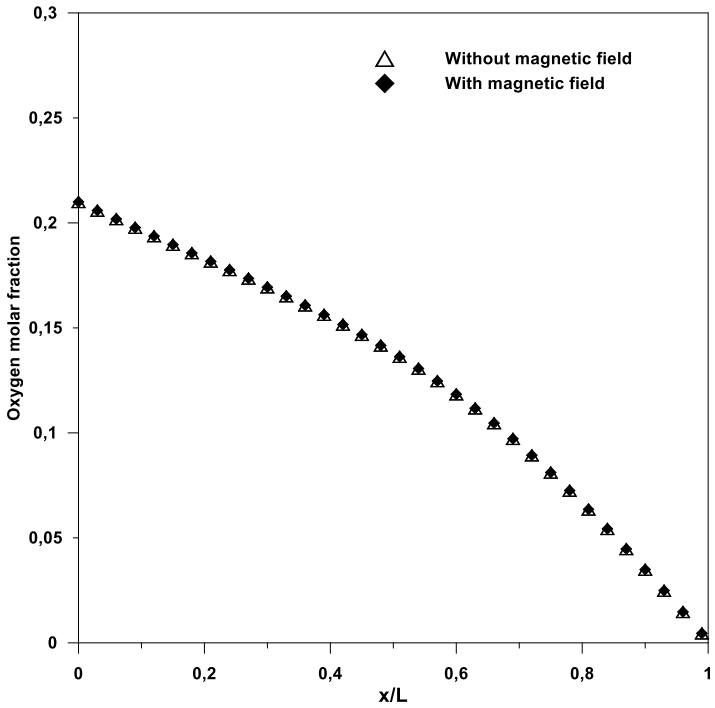

Figure 6. Effect of Kelvin force on the distribution of oxygen molar fraction.

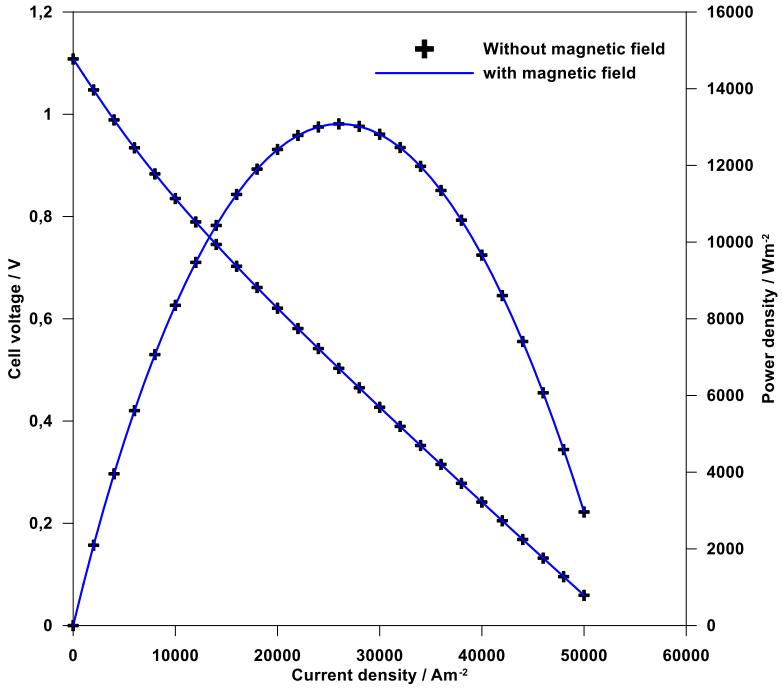

Figure 7. Kelvin force effect on SOFC performance

ISBN: 978-1-63248-189-4 DOI: 10.15224/978-1-63248-191-7-01

References

[1] R.J. Gorte, "Recent developments towards commercialization of solid oxide fuel cells", AIChE Journal, vol. 51, pp. 2377–2381, 2005.

[2] A. Atkinson, S. Barnett, RJ. Gorte and al. "Advanced anodes for high-temperature fuel cells", Nat Mater, vol. 3, pp.17–27, 2004.

[3] AD. Aljaberi, JTS .Irvine, "Ca-substituted, A-site deficient perovskite La0.2Sr0.7TiO as a potential anode material for SOFCs", J Mater Chem A, vol. 1, pp. 5868, 2013.

[4] AA. Reddy, A. Goel, DU. Tulyaganov and al., "Thermal and mechanical stability of lanthanide-containing glass–ceramic sealants for solid oxide fuel cells". J Mater Chem, vol. A 2, pp.1834–1846, 2014.

[5] SH. Jensen, X. Sun, SD. Ebbesen and al., "Pressurized operation of a planar solid oxide cell stack", Fuel Cells, vol.16, pp.205–218, 2016.

[6] TS. Li, M. Xu, C. Gao and al. "Investigation into the effects of sulfur on syngas reforming inside a solid oxide fuel cell", J Power Sources, vol. 258, pp. 1–4, 2014.

[7] M. Xu, B. Li, B. Wang and al., "Mechanism of phosphorus and chlorine passivating a nickel catalyst: a density functional theory study", Electrochim Acta, vol. 167, pp. 147–150, 2015.

[8] Y. Chen, W. Zhou, D. Ding and al., "Advances in cathode materials for solid oxide fuel cells: complex oxides without Alkaline earth metal elements", Adv Energy Mater, vol. 5, pp. 1500537, 2015.

[9] Y. Chen, Y. Lin, Y. Zhang and al., "Low temperature solid oxide fuel cells with hierarchically porous cathode nano-network", Nano Energy, vol. 8, pp. 25–33, 2014.

[10] M. Andersson, J. Yuan and B. Sunden, "SOFC cell design optimization using the finite element method based CFD approach". Fuel Cells, vol. 14, pp. 177–188, 2014.

[11] D. Chen, Q. Zhang, L. Lu and al., "Multi scale and physics models for intermediate and low temperatures H^+ -solid oxide fuel cells with $H^+/e^-/O^{2-}$ mixed conducting properties: part A, generalized percolation theory for LSCF-SDC-BZCY 3-component cathodes", J Power Sources, vol. 303, pp. 305–316, 2016.

[12] K. Ruksawong, R. Songprakorp and al., "Investigation of PEMFC under Static Magnetic Field: Temperature, Relative Humidity and Performance", Journal of The Electrochemical Society, vol. 164 (2), pp. F1-F8, 2017.

[13] H. Matsushima, T. Iida, Fukunaka. Y and A. Bund. "PEMFC Performance in a Magnetic Field", FUEL CELLS, vol. 08, pp. 33–36, 2008.

[14] MA. Khaleel, Z. Lin, P. Singh, W. Surdoval and D. Collin. "A FEA modelling tool for SOFC development: coupled electrochemistry, thermal and flow analysis in MARC", J Power Sources, vol. 130, pp. 136-48, 2004.

[15] K. Tseronis, I. Bonis, IK. Kookos and C. Theodoropoulos, "Parametric and transient analysis of non-isothermal, planar SOFCs", Int J Hydrogen Energy, vol.37, pp. 530-47, 2012.

[16] VM. Janardhanan and O. Deutschmann, "Modeling diffusion limitation in solid-oxide fuel cells", Electrochim Acta ,vol. 56, pp. 9775–9782, 2011.

[17] M. Ni, "Modeling and parametric simulations of solid oxide fuel cells with methane carbon dioxide reforming", Energy Convers Manag, vol. 70, pp. 116–129, 2013.

[18] Y. Xie and X. Xue, "Multi-scale electrochemical reaction anode model for solid oxide fuel cells", J Power Sources, vol. 209, pp. 81–89, 2012.

[19] S. Chen and GD. Doolen, "Lattice Boltzmann method for fluid flows", Annu Rev Fluid Mech, vol. 30,pp. 329-64, 1998.

[20] AA. Mohammad, "Applied lattice Boltzmann method for transport phenomena momentum heat and mass transfer", The University of Calgary Press, 2007.

[21] L. Chen, Q. Kang, Y. He and W. Tao, "Pore-scale simulation of coupled multiple physicochemical thermal processes in micro reactor for hydrogen production using lattice Boltzmann method", International Journal of Hydrogen Energy, vol. 37, pp. 13943-13957, 2012.

[22] P. Asinari, MC. Quaglia, MR. Spakovsky and BV. Kasula, "Direct numerical calculation of the kinematic tortuosity of reactive mixture flow in the anode layer of solid oxide fuel cells by the lattice Boltzmann method", J Power Sources, vol. 170(2), pp. 359-75, 2007.

[23] X. Han, D. Zheng and, B. Bo-Feng, "Electrochemical performance study of solid oxide fuel cel3 using lattice Boltzmann method". Energy, vol.67, pp. 575-583, 2014.

[24] X. Han and D. Zheng, "Lattice Boltzmann modeling of carbon deposition in porous anode of a solid oxide fuel cell with internal reforming", Applied Energy, vol. 178, pp. 294–307, 2016.

[25] S. Kakaç, A. Pramuanjaroenkij andXY. Zhou, "A review of numerical modeling of solid oxide fuel cells", J Hydrog Energy, vol. 32, pp. 761–786, 2007.

[26] Fuel cell handbook. seventh ed. Morgantown, (WV, USA): EG & G Technical Services Inc., U.S. Department of Energy; November 2004. p. 57e60.

[27] Y. Abir and al, "Electrochemical performance of solid oxide fuel cell: Experimental study and calibrated model", Energy, vol. 142, pp. 932-943, 2018.

[28] N. Meng, "2D thermal-fluid modeling and parametric analysis of a planar solid oxide fuel cell. Energy Conversion and Management", vol. 51, pp. 714-721, 2010.

[29] JL. Yuan, XR. Lv, B. Sunden and DT. Yue, "Analysis of parameter effects on transport phenomena in conjunction with chemical reactions in ducts relevant for methane reformers". Int J Hydrogen Energy, vol. 32, pp. 3887–98, 2007.

[30] SG. Neophytides, "The reversed flow operation of a crossflow solid oxide fuel cell monolith", Chemical Engineering Science, vol. 54, pp. 4603–13, 1999.

[31] B. Zitouni, H. Ben Moussa, K. Oulmi, S. Saighi and K. Chetehouna, "Temperature field, H_2 and H_2O mass transfer in SOFC single cell: Electrode and electrolyte thickness effects", International journal of hydrogen energy, vol. 34, pp. 5032–5039, 2009.

ISBN: 978-1-63248-189-4 DOI: 10.15224/978-1-63248-191-7-01

[32] A. Lazzaretto and A. Toffolo, “Energy, economy and environment as objectives in multi-criterion optimization of thermal systems design”, Energy, vol. 29, pp. 1139–57, 2004.

[33] P. Mandin, C. Bernay, S. Tran-Dac, A. Broto, D. Abes and M. Cassir, “SOFC modelling and numerical simulation of performance”, J Fuel Cells, vol. 6(1), pp. 71–8, 2006.

[34] P. Aguiar, CS. Adjiman and NP. Brandon, “Anode supported intermediate temperature direct internal reforming solid oxide fuel cell. I: model based study state performance”, J Power Sources, vol. 138, pp. 120–36, 2004.

[35] N. Meng, KHL. Michael and YCL. Dennis, “Parametric study of solid oxide fuel cell performance”, Energy conversion and management, vol. 48, pp. 1525-1535, 2007.

[36] H. Bai, P.Yu, H. Winoto and H.T. Low, “Lattice Boltzmann method for flows in porous and homogenous fluid domains coupled at the interface by stress jump”, International Journal for Numerical Methods in Fluids, vol. 60, pp. 691-708, 2009.

[37] W. Jinku, “A lattice Boltzmann algorithm for fluid-solid conjugate heat transfer”, Inetrantional Journal of Thermal Sciences, vol.10, pp. 228-234, 2007.

[38] X. Shan and H. Chen, “Lattice Boltzmann model for simulating flows with multiple phases and components”, Phys Rev E, vol. 47, pp. 1815-1820, 1993.

[39] WP. Rogers, RS. Gemmen, C. Johnson, M. Prinky, M. Shalhnam, “Validation and application of CFD-based model for SOFCs and stacks”, ASME, 2003.

[40] L.D. Landau and E.M. Lifshitz, “Electrodynamics of Continuous Media. Pergamon”, Oxford,Chapter 4, 1960.

[41] T. Okaba, N.I. Wakayama, L. Wang, H. Shingu, J.I. Okano and T. Ozawa, “The effect of magnetic field on the oxygen reduction reaction and its application in polymer electrolyte fuel cells”, Electrochimica acta , vol. 48, pp. 531-539, 2003.

[42] K. Yamakawa, K. Okawa and K. Miyanoto, “Design of Permanent Magnet and Their Application”, Sogodenshi Publishing Co. Ltd., p. 89, 1992.

[43] L.B. Wang, N.I. Wakayama and T. Okada, “Numerical simulation of enhancement of mass transfer in the cathode electrode of a PEM fuel cell by magnet particles deposited in the cathode-side catalyst layer”, Chemical Engineering Science, vol. 60, pp. 4453–4467, 2005.